analytical chemistry

Article

A Rapid SARS-CoV-2 Nucleocapsid Protein Profiling Assay with High Sensitivity Comparable to Nucleic Acid Detection

Jie Liu, Jinpeng Mao,* Mengyu Hou, Zhian Hu, Gongwei Sun, and Sichun Zhang*

Cite This: *Anal. Chem.* 2022, 94, 14627−14634

Read Online

ACCESS | Metrics & More | Article Recommendations | Supporting Information

ABSTRACT: Existing nucleic acid and antigen profiling methods for COVID-19 diagnosis fail to simultaneously meet the demands in sensitivity and detection speed, hampering them from being a comprehensive way for epidemic prevention and control. Thus, effective screening of COVID-19 requires a simple, fast, and sensitive method. Here, we report a rapid assay for ultrasensitive and highly specific profiling of COVID-19 associated antigen. The assay is based on a binding-induced DNA assembly on a nanoparticle scaffold that acts by fluorescence translation. By binding two aptamers to a target protein, the protein brings the DNA regions into close proximity, forming closed-loop conformation and resulting in the formation of the fluorescence translator. Using this assay, saliva nucleocapsid protein (N protein) has been profiled quantitatively by converting the N protein molecule information into a fluorescence signal. The fluorescence intensity is enhanced with increasing N protein concentration caused by the metal enhanced fluorescence using a simple, specific, and fast profiling assay within 3 min. On this basis, the assay enables a high recognition ratio and a limit of detection down to 150 fg mL^{-1}. It is 1−2 orders of magnitude lower than existing commercial antigen ELISA kits, which is comparative to or superior than the PCR based nucleic acid testing. Owing to its rapidity, ultrasensitivity, as well as easy operation, it holds great promise as a tool for screening of COVID-19 and other epidemics such as monkey pox.
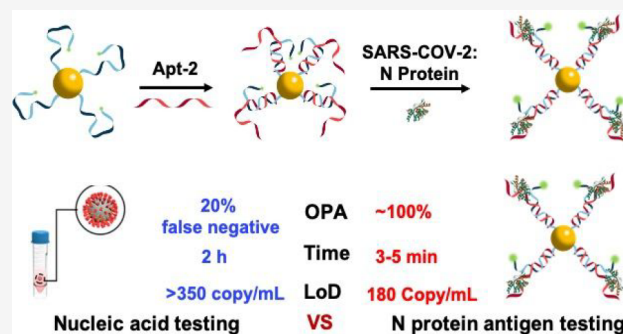
INTRODUCTION

The spread of COVID-19 pandemic, caused by SARS-CoV-2 across the world, represents the greatest challenge to human health.[1−3] Rapid diagnosis of the COVID-19 virus is among the foremost priorities in prevention and control of the current epidemic.[4,5] Nucleic acid-based analysis such as quantitative reverse transcription polymerase chain reaction (qRT-PCR) has been regarded as a gold standard for clinical diagnoses of COVID-19 pathogens.[6−8] However, there are still about 20−30% of false-negative results caused by improper sample collection pathways.[9] In addition, the current approach requires complex extraction and amplification procedures, which are mostly conducted in centralized laboratories with skilled operators, specialized facilities, and a long reaction time up to 2−4 h.[6,10−12] The long turnaround times have prompted the need for an alternative screening tool for viral testing that is rapid, simple, sensitive, and straightforward for point-of-care or even at-home testing.[11,13]

Antigen testing is another common COVID-19 diagnostic method.[14−16] The advantages of rapid and easy operation make it possible for real time detection of the COVID-19 virus.[17] Elevated levels of antigen are an early indicator of multiple pandemics; for example, the recently reported severe acute hepatitis in children was associated with the SARS-CoV-2 superantigen.[18] The antigenic proteins of SARS-CoV-2 include nucleocapsid (N), spike (S), membrane, and envelope proteins.[19] Among these, the N protein plays a major role in the synthesis and translation steps of virus RNA.[9,20] It also provides higher sensitivity when it is used as a target protein due to its high immunogenicity compared to that of S protein.[21] It is worth noting that the amount of antigenic protein content in a single virus particle can be thousands of times more than the nucleic acid content.[22,23] Additionally, it would release large amounts of free N protein without nucleic acid in its early stage of viral replication; nucleic acid negative samples may also be antigen-positive.[24,25] Therefore, in comparison to S protein, elevated concentration of N protein is of great importance for the early diagnosis and control of COVID-19.[6] However, the low sensitivity of the commercial antigenic ELISA kit faces the risk of false negatives for low abundance N protein profiling. Direct N protein testing with high sensitivity is still difficult in COVID-19 screening.

To date, most of the published N protein profiling methods are immunoassays.[26] Traditional immunoassay employs multi-
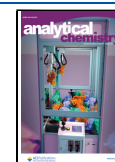
Scheme 1. Schematic Illustration of Fabrication of the Binding-Induced DNA Assembly Assay for the Profiling of the N Protein[a]
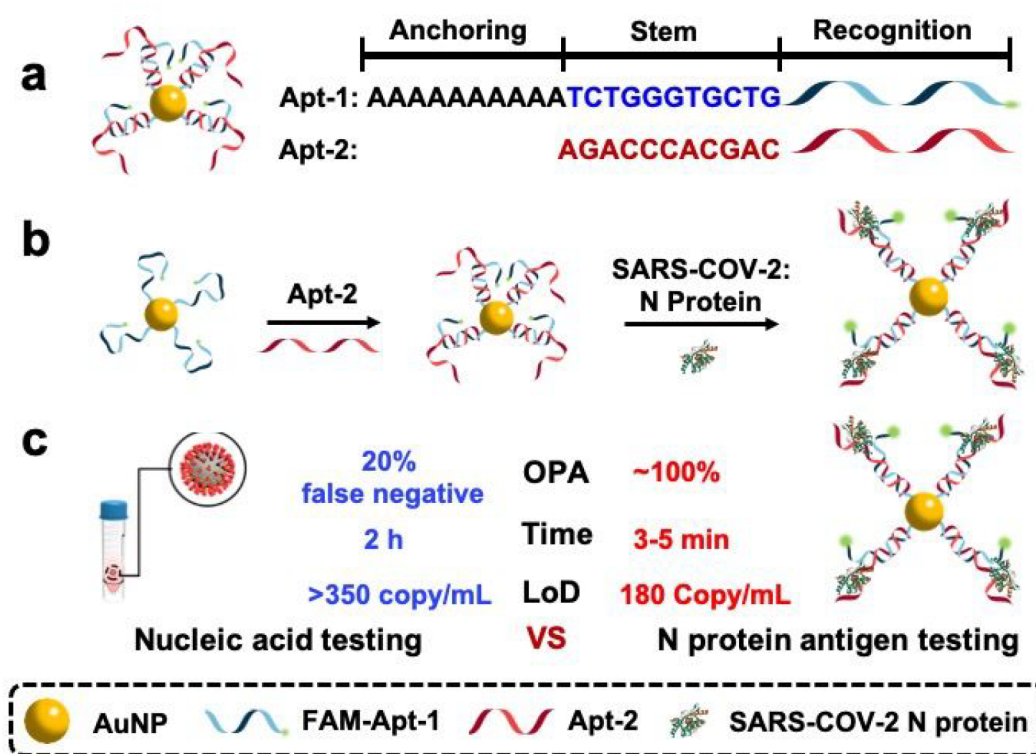
[a](a) Conformation of the two aptamers on the surface of AuNP. (b) Fluorescence assay for the synchronous recognition of N protein by binding-induced two-aptamer assembly. (c) Performance comparison between the nucleic acid testing and the assay-based N protein antigen testing.

ple reagent incubation and washing steps, which are imperfect for real-time detection of N protein due to its time-consuming and complicated operation.[9] To troubleshoot the problem, DNA-based affinity sensing strategies are emerging as viable alternatives to antibody-based immunoassays.[27−29] Advances in DNA assembly and affinity binding have enabled exciting developments of nanosensors.[30] For a specific analyte with the DNA nanostructure, translation of the input target into a unique output DNA to trigger the following assembly is one of the key steps.[31] Thus, many efforts have been directed to molecular translators based on DNA assembly.[32−34] Biosensors based on the structural switching of aptamers and other DNA-based structures containing recognition elements have been applied to biomacromolecule detection or inhibited SARS-CoV-2 virus infection.[35−37,11] Binding of two aptamers to the same target was able to selectively detect the analyte even at a very low concentration.[38] As a promising assay platform, advances in gold nanoparticle (AuNPs) and its unique optical properties will be exploited and incorporated in detection schemes, further broadening the utility of the binding-induced assembly for target profiling.[30,31,39−41] With rational design of the surface chemistry of AuNPs by modified target binding-induced aptamer assembly, the strategy can potentially be utilized to design a molecular translator for N protein profiling. Some smart strategies for transforming aptamer−S protein interactions into electrochemical signals has been reported.[42] Even so, fluorescence-based signal transduction is more powerful because such strategies may be utilized to translate aptamers into a real-time optical nanosensor, which provided a potential way for an N protein point-of-care test.[43,44]

Here, we report a direct N protein profiling fluorescence assay that acts by binding-induced DNA assembly. Depending on the synchronous recognition of N protein via two aptamers, enhanced profiling specificity and sensitivity were achieved. The binding-induced fluorescence assay is composed of target-recognition and signal-output elements (Scheme 1). The recognition process was designed based on assembly of N protein's two aptamers (Apt-1 and Apt-2) on AuNPs. As shown, the first aptamer (FAM labeled Apt-1) was confined onto the surface of AuNP via Poly 10A and serves as the scaffold of the probe. The second aptamer (Apt-2) was partly hybridized with Apt-1 to form a stable stem duplex. Thus, in the absence of the analyte, the fluorescence of the system is minimal, thus resulting in very little background. In the presence of the N protein, the two aptamers are brought into close proximity, forming a closed-loop conformation, resulting in the formation of the fluorescence translator. The fluorescence intensity was enhanced with increasing N protein concentration caused by the metal enhanced fluorescence. Owing to the synergy effect of the two aptamers simultaneously targeting the N protein, the assay has a higher recognition ratio toward N protein in saliva testing samples. The average diagnostic time reaches ∼3 min, much faster than existing technologies of nucleic acid assays. The signals of this method can be easily recorded using a microplate reader with high sensitivity by only recording the fluorescence intensity at 524 nm without relying on other sophisticated instruments. This work provides the foundation for the development of simple devices facilitating on-demand COVID-19 detection.
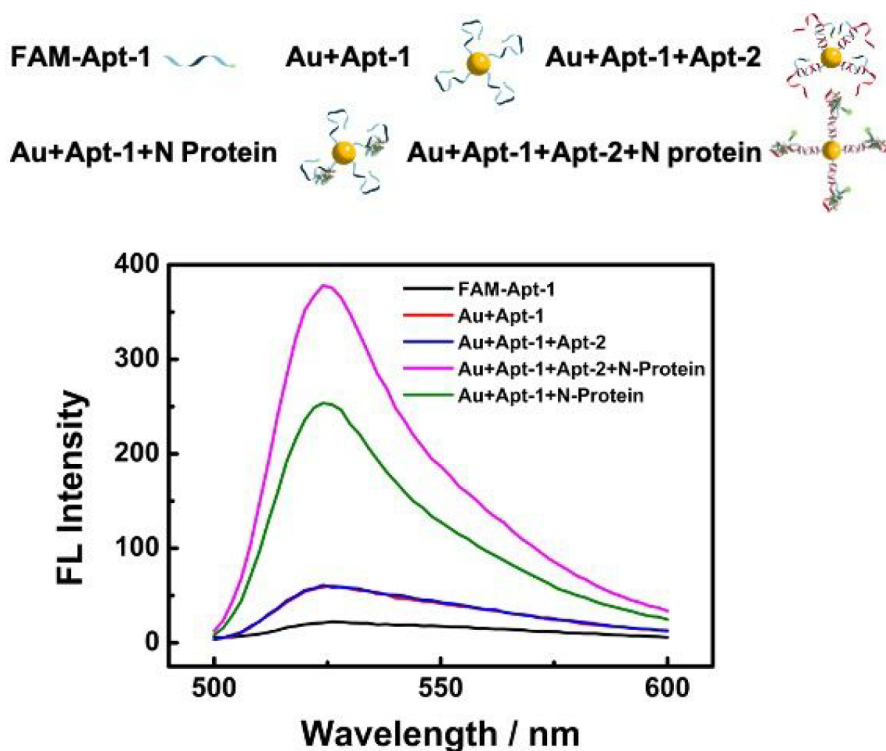
Figure 1. Fluorescence emission spectra (λ_{em} = 524 nm) of Apt-1 in the presence of different mixture systems.

■ EXPERIMENTAL SECTION

Chemicals and Materials. All chemicals and materials used in this work are described in the Supporting Information.

Fabrication of the Binding-Induced Fluorescence Translator. The principle of this experiment involves binding of Apt-1 functionalized AuNPs with Apt-2 to N protein. Typically, Apt-1 (20 μL of 1.0 μM) and Apt-2 (20 μL of 1.0 μM) was dissolved in PBS, and then the solution was heated to 95 °C and maintained for 10 min, followed by cooling to room temperature as slowly as possible for complete hybridization to the partly complementary sequences of the two aptamers. Second, the above solution was added to the AuNPs solution (molar ratio of Apts/AuNPs, 20:1), and the mixture was shaken for another 15 min. The mixture solution was further treated with BSA (w/v, 0.5%) if necessary for 10 min at 37 °C to passivate the excess active sites on the surface of AuNPs. Finally, the mixture was centrifuged and washed three times with PBS. The resulting binding-induced DNA assembly assay-based probe was used for profiling proteins. The binding-induced fluorescence translator was then used as the probe for N protein profiling.

Characterization of the Binding-Induced Fluorescence Translator. The synthetic AuNPs showed an average diameter of about 13 nm. After the AuNPs were functionalized with two aptamers, the characteristic peak of aptamers at 260 nm was significantly increased (Figure S1a). In addition, the dynamic light scattering (DLS) experiments showed that the average hydrodynamic size increased by about 8−10 nm (Figure S1b) after two aptamers were decorated on to the surface of AuNPs. In addition, zeta-potential analysis indicated that the Apts/AuNPs had a more negative zeta potential (−45.8 mV) compared to the bare AuNPs (−23.8 mV) (Figure S1c). Because AuNPs and aptamers were negatively charged, a higher aptamer concentration should result in a more negatively charged surface. The result further confirmed that the AuNPs were successfully assembled with two aptamers.

Assembly of Aptamers on Gold Electrode. In the mechanism test procedure, two aptamers of N protein were fabricated on a gold working electrode. Briefly, ferrocene was conjugated to the 5′-end of the Apt-1 and was then partly hybridized with Apt-2. Prior to modification of the electrodes, aptamer stock solution (0.02 mM) was reduced in 10 mM TCEP for 1 h to cleave disulfide bonds. This solution was then diluted in HEPES buffer to achieve the desired aptamer concentration (about 0.5−8 μM). For aptamer immobilization, the gold electrodes were kept in a solution of thiolated aptamer for 16 h in the dark at 4 °C. The electrode surfaces were then passivated by incubating in a 3 mM MCH solution for 1 h.

N Protein Detection Using the Binding-Induced Fluorescence Translator. In the N protein detection step, the developed probes were incubated with N protein (10 μL) in a series of concentrations in phosphate buffer, respectively. The final solutions were diluted to 200 μL. Fluorescence spectra measurements were thereafter performed after another 3−5 min incubation, and every experiment was performed in triplicate. The only difference between the sensing assays is the concentration of N protein.

N Protein ELISA. ELISAs on saliva samples were performed in our laboratory with slight modification to the manufacturer's suggested protocol to minimize systematic bias between ELISA and the designed assay's result. The assay volumes and liquid handling techniques were matched as closely as possible. The standard curve dilution series was matched to that used in the developed assays. Saliva and N protein standard curve samples were loaded and analyzed in triplicate.

RESULTS AND DISCUSSION

To test the feasibility of the designed probe for N protein analysis, the fluorescence spectra of Apt-1 (100 nM) in the presence of different mixture systems were tested. AuNPs here were utilized as the nanocarriers and fluorescent enhancer, since they possess many properties, including distance-dependent optical features, protecting oligonucleotides from degradation.[45] Phosphate buffer solution (PBS, 10 mM) containing 40 pg/mL N protein was used as the target protein. The assay was incubated with the N protein at room temperature for 3−5 min. Then the fluorescence intensities of bare Apt-1, Apt-1 decorated AuNPs, binding-induced DNA assembly assay, and assay in the presence of N protein were recorded. As shown in Figure 1, bare FAM fluorescein labeled Apt-1 exhibited negligible fluorescence intensity. Apt-2 was partly hybridized with Apt-1 to form a stable partly hybridized FAM-Apt-1/Apt-2 duplex ($T_m \approx 40$ °C), which was immobilized on the surface of AuNPs, resulting in a slight enhancement of the fluorescence due to the metal enhanced fluorescence (MEF),[46] which was comparable to the that of Apt-1 decorated AuNPs, indicating that without the N protein, binding-induced DNA assembly was inactive. Upon addition of N protein, the binding of N protein to Apt-1 and Apt-2 enables the two aptamers to recognize protein by forming a closed-loop conformation. The fluorescence of the mixture was remarkably increased with nearly multifold enhancement. The enhancement was superior to the assay without Apt-2. This was because there was no binding-induced DNA assembly occurring in the absence of Apt-2 (green curve). These results demonstrated that the binding-induced DNA assembly assay could be used as a potential assay for N protein profiling.

To confirm that the fluorescence enhancement was ascribed to the change of distance-dependent AuNP surface chemistry induced by the N protein binding, electrochemical detection of N protein using aptamer-modified gold electrodes was conducted. The demonstrated strategy pursued in this study involved self-assembly of thiolated Apt-1 partly hybridized with Apt-2 on gold electrode surfaces (Figure 2a). The change in redox current was determined using differential pulse voltammetry. The binding of N protein caused the closed-loop conformation between the two aptamers and the N protein, decreasing the efficiency of electron transfer from the redox label (5′ of Apt-1, ferrocene) to the gold electrode as shown in Figure 2b.[47] This result demonstrated that the target binding-induced aptamer assembly changed the distance between the redox label and the gold electrode.[48] Similarly, as for the designed fluorescence assay, after the N protein binding, the distance between the FAM and AuNPs was also extended,[49] thus resulting in enhancement of the fluorescence intensity. A control probe functioned with the duplexes of Apt-3/Apt-4 (see Table S1) which lacked the N protein aptamer sequences (replaced by other types of aptamers) was used for the profiling the N protein, only a negligible fluorescence enhancement of FAM was observed in the control group as shown in Figure S2. These results further confirmed that the fluorescence enhancement was related with the N protein binding-induced aptamer assembly.

To evaluate the sensitivity of the newly designed assay for N protein profiling, the surface chemistry of AuNPs was first optimized, since the coverage of aptamers on the surface of AuNPs may affect the performance of the assay. The length of stem sequences, the number of bases of polyA, the incubation
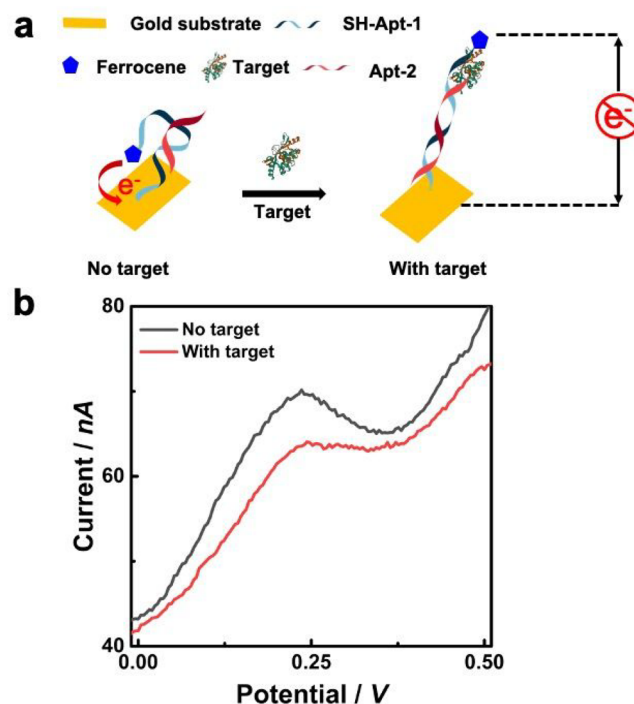
Figure 2. Aptamer-based electrochemical analysis of distance depended on changing surface chemistry. (a) The Apt-1 was thiolated at the 3′ end and partly assembled with Apt-2 on gold electrodes. The redox label was attached at the 5′ end of Apt-1 and was in close proximity to the electrode surface. Upon addition of target, the changed conformation made the redox label move further away from the electrode, lowering the electron-transfer efficiency. (b) The differences in Faradaic current before and after addition of N protein were quantified using differential pulse voltammetry.

time, and the volume of AuNPs were optimized, as shown in Figures S3−S6, respectively. Then, PBS containing the binding-induced DNA assembly assay has been treated with different concentrations of N protein. Figure 3a exhibited the fluorescence intensity of bare Apt-1 modified AuNPs for N protein profiling from 0.5 pg mL^{-1} to 0.1 ng mL^{-1}. The fluorescence intensity at 524 nm exhibited a bad linear correlation with the concentration of N protein as shown in Figure 3b. In comparison, the fluorescence intensity of the binding-induced DNA assembly assay increased with the addition of N protein from 0.5 pg mL^{-1} to 0.1 ng mL^{-1} as shown in Figure 3c. The fluorescence intensity at 524 nm exhibited a linear correlation with the concentration of N protein. The better sensitivity was contributed by the synergy effect of the two aptamers simultaneously targeting N protein.[50,51] In the presence of Apt-2, the binding-induced two aptamer assembly has a higher recognition ratio toward N protein than bare Apt-1. This result wonderfully verified the feasibility of the assay for N protein profiling. The linear equation is $F = 2.35C + 132.25$ with a correlation coefficient (R^2) of 0.985 as shown in Figure 3d, where C is the concentration of N protein in PBS, F is the fluorescence intensity of FAM at 524 nm. On the basis of $3\sigma/k$ (σ, the standard deviation of the blank sample; k, the slope of the standard curve), the limit of detection (LOD) of N protein was calculated to be ca. 190 fg mL^{-1}. Indicating that the assay could quantitate N protein at a very low concentration, which is comparative to or superior than the commercial antigen ELISA Kit. Overall, as shown in Table S2, the proposed
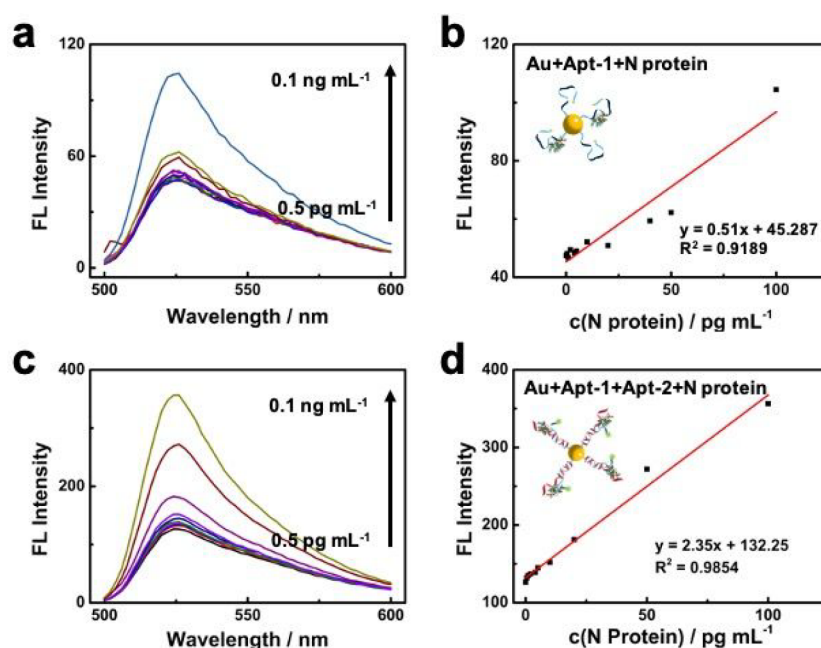
Figure 3. Detection of N protein concentration in phosphate buffer with two different profiling assays. (a) Fluorescence emission spectra of bare Apt-1 modified AuNPs in response to different concentrations of N protein. (b) Relationship between the fluorescence intensity to different concentrations of N protein. (c) Fluorescence emission spectra of the binding-induced DNA assembly assay in response to different concentrations of N protein. (d) Relationship between the fluorescence intensity to different concentrations of N protein.
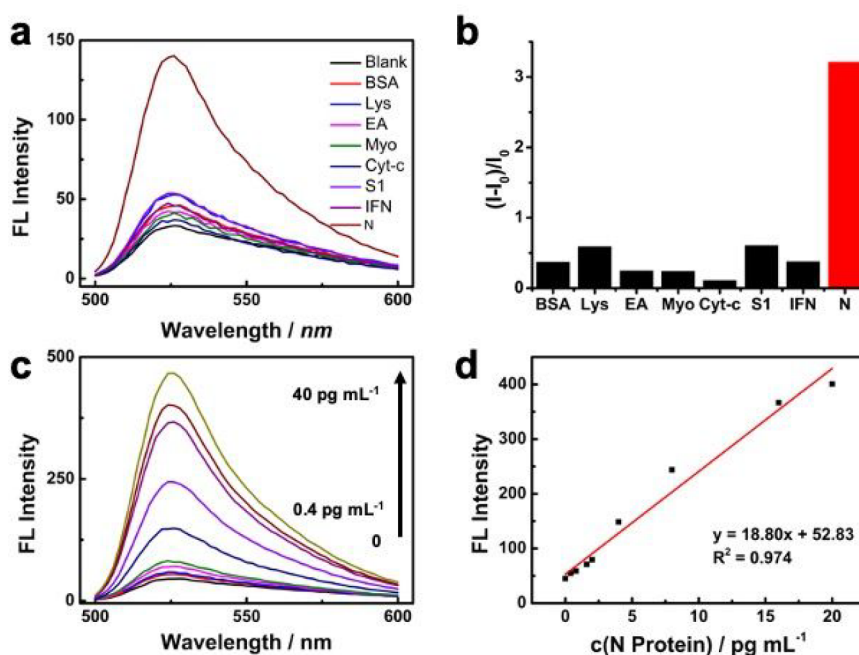
Figure 4. Profiling of N protein concentration in human saliva. (a) Fluorescence emission spectra of the binding-induced DNA assembly assay in response to different kind of proteins. (b) Fluorescence intensity ratio $(I - I_0)/I_0$ of the binding-induced DNA assembly assay in PBS containing the N protein (80 pg mL^{-1}) and other nontarget proteins (S1 protein: 4.0 μg mL^{-1}, others: 1.0 μg mL^{-1}). (c) Fluorescence emission spectra of the binding-induced DNA assembly assay in response to different concentrations of N protein added in human saliva. (d) Relationship between the fluorescence intensity to different added N protein concentration in human saliva.

method in this work exhibits a better sensitivity compared with other assay methods.

The specificity of the binding-induced DNA assembly assay for N protein profiling has also been verified by using various interference proteins, including bovine serum albumin (BSA), egg albumin (EA), myohemoglobin (Myo), lysozyme (Lys),

cytochrome c (Cyt-c), and SARS-CoV-2 S1 protein (S1). The concentration of N protein and S1 protein is 80 pg mL^{-1} and 4.0 μg mL^{-1}, respectively. Those of all other proteins are 1.0 μg mL^{-1}. S1 protein exists on the surface of virus particles, which is closely related to the pathogenesis of COVID-19 as well as N protein. As shown in Figure S7, satisfactory

specificity of the assay for N protein detection was achieved. Under the same conditions the fluorescence intensities of these interference proteins are very low even though their concentrations are much higher than that of N protein, suggesting satisfactory specificity of the assay for N protein profiling. The binding-induced DNA assembly assay is dependent on synchronous recognition of N protein via two aptamers with enhanced specificity. In contrast, the specificity of bare Apt-1 modified AuNPs for N protein profiling was also conducted as shown in Figure S8. The fluorescence response of S1 protein was equal to the that of N protein. The assay based on bare FAM-Apt-1 modified AuNPs restricted its specificity performance. These results suggest satisfactory specificity of the developed binding-induced DNA assembly assay for N protein profiling.

The clinical applicability of the as-prepared assay was further investigated by profiling N protein in human saliva using the standard curve method. Healthy saliva samples were collected from volunteers who were forbidden to eat or drink for 2 h prior to the collection. After centrifugation for about 5 min at 12,000 rpm, the precipitates were discarded, and the supernatant was stored at −20 °C for further use. We first evaluated the selectivity of the assay to other nontarget proteins and the response in human saliva containing 80 pg mL^{-1} N protein. Satisfactory specificity of the assay for N protein detection was achieved as shown in Figure 4a and b. The binding-induced DNA assembly assays are dependent on the synchronous recognition of N protein via two aptamers with enhanced specificity. Then, different concentrations of N protein (0.4, 0.8, 1.6, 2, 4, 8, 16, 20, 40 pg mL^{-1}) were added into diluted saliva. The fluorescence response of the assay toward saliva diluted with N protein was then evaluated. The assays were incubated with the saliva mixture for 5 min. As shown in Figure 4c, the fluorescence emission of FAM was enhanced with the increase of the N protein concentration. Figure 4d reveals the linear correlation between fluorescence intensity and the concentration of the N protein. The linear equation is $F = 18.80C + 52.83$ with a correlation coefficient (R^2) of 0.974, where C is the concentration of N protein added in saliva, F is the fluorescence intensity of FAM at 524 nm. On the basis of $3\sigma/k$, the limit of detection (LoD) of N protein was calculated to be about 150 fg mL^{-1} (equivalent to 180 copy/mL), which was comparative to or superior than the PCR based nucleic acid testing (600−3200 copy/mL) and 1−2 orders of magnitude higher than existing commercial antigen ELISA Kit. Table S3 presents that the recoveries ranging from 95.4% to 103.3%. These results demonstrated that the developed assay possesses great practicability in clinical human saliva samples for sensitive N protein profiling.

Additionally, the relative added N protein concentration in human saliva was calibrated by enzyme-linked immunosorbent assay using the commercial ELISA standard curve. The N protein concentrations were chosen to cover the range suggested by the ELISA kit (5, 10, 20, 50, 100, and 200 pg mL^{-1}, respectively). A linear relationship between optical density at 450 nm and standard N protein concentration was conducted using the kit by weighted least-squares regression analysis ($R^2 = 0.999$) and the saliva used was diluted 10-fold beyond the requirements for ELISA. Furthermore, human saliva was then supplemented with incremental N protein concentrations and calibrated against N protein using the standard curve achieved above as shown in Figure 5. Based on the standard curve achieved in Figure 4d, the corresponding
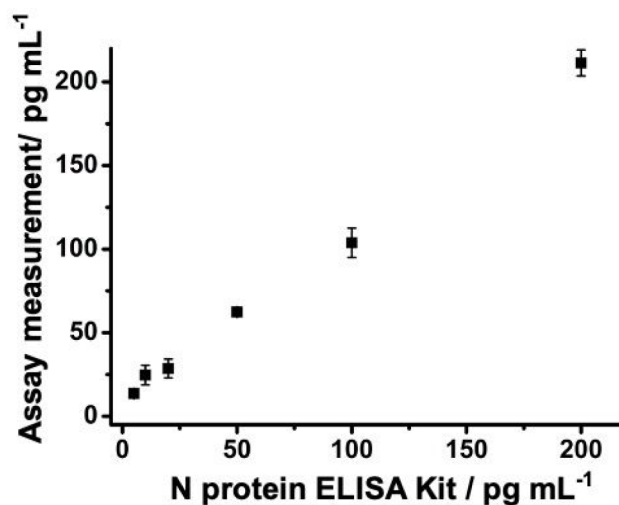
Figure 5. Comparison of assay accuracy with a commercial ELISA kit. N protein assay results using human saliva from healthy volunteers was supplemented with purified N protein to simulate samples covering the range of a commercial ELISA kit. Data are plotted as regressed value ±95% confidence intervals. The short solid line represents 1:1 agreement between supplemented N protein and designed assay-regressed N protein.

concentration that the binding-induced DNA assembly assay determined by the relative fluorescence intensity was 13.69, 24.63, 28.58, 62.36, 103.82, and 211.35 pg mL^{-1}, respectively. Results from this designed assay consistently agreed with the known N protein concentration within 95% confidence limits. To confirm the stability for N protein profiling in different human saliva samples, the assay was also used on men's and women's saliva, respectively. As shown in Figure S9, the fluorescence intensity of the assay was different between men and women, while it exhibited nearly the same fluorescence intensity in the same gender. These results indicated that the designed assay could discriminate different N protein concentrations among different human saliva in biomedical applications.

To validate the versatility of the assay, the binding-induced DNA assembly assay could also be used to establish a simple fluorescence method for the detection of alternative bio-macromolecules. It is interesting that the interferon, such as interferon gamma (IFN γ), the body's main defense, actually helps SARS-CoV-2 attack the human immune system.[52] Thus, elevated levels of IFN γ with high simplicity and reliability is of great importance. By changing the two aptamers to Apt-7 and Apt-8 (Table S1), extracts from human cervical cancer cells (HeLa) were used as the source of IFN γ. The binding-induced DNA assembly assay was incubated with the cell extracts of different concentrations at 37 °C for 60 min, and then the fluorescence spectra were recorded. As can be seen from Figure S11, when the number of HeLa cells was raised from 0 to 10,000 in the reaction system, the fluorescent intensity of the assay showed an obvious enhancement. Further studies were supplemented to supporting the MEF mechanism. As shown in Figure S12, the fluorescence time traces of FAM-Apt-1 and AuNP-FAM-Apt-1/Apt-2+N protein both exhibited single-step photobleaching characteristics, proving that the luminescence points are FAM dye molecules. Compared with the individual FAM molecule (Figure S12A), the fluorescence intensity of the FAM molecule after the construction of the AuNP sensing platform (Figure S12B) was significantly

enhanced by about 4.76 times, exhibiting enhanced photobleaching resistance time (ca. 1.5−2.7 s), which directly confirms that the MEF effect is significant. These results suggest that the binding-induced DNA assembly assay could be extended as a universal method for the detection of other biomacromolecules which have two recognition elements.

CONCLUSION

In summary, we report a direct SARS-CoV-2 nucleocapsid protein testing methodology based on a binding-induced DNA assembly fluorescence assay. By taking advantage of binding-induced two-aptamer assembly and AuNPs causing metal enhanced fluorescence, the sensitive profiling of N protein in human saliva was achieved. An urgent issue that COVID-19 testing faces, the trade-off between sensitivity and the speed of the report, was addressed. Compared with other methods, the binding-induced DNA assembly assay has excellent performance in terms of testing time and sensitivity. The test time (<3 min) is much faster than the existing nucleic acid testing technologies such as qRT-PCR (25−420 min), RT-LAMP (15−60 min), CRISPR (>20 min), electrochemistry (<120 min), and commercial ELISA kits. The LOD reaches 150 fg mL^{-1} (equivalent to 180 copy/mL), at least 20-fold lower than the U.S. Centers for Disease Control and Prevention (CDC)/ China National Medical Products Administration (NMPA)-approved qRT-PCR assays (0.6−3.2 copies μL^{-1}), thus making the assay attractive for potential point-of-care applications. The concept and strategy reported herein can also be applied to construct binding-induced molecular translators for other molecular targets. It holds great promise as a comprehensive tool for population-wide screening of COVID-19 and other epidemics such as monkey pox.

ASSOCIATED CONTENT

Ⓢ Supporting Information

The Supporting Information is available free of charge at https://pubs.acs.org/doi/10.1021/acs.analchem.2c02670.

> Chemicals and materials; Preparation of gold nanoparticles; Cell culture and IFN γ extraction; Detection of IFN γ in cell extracts; List of detailed DNA sequences used in this study; Comparison of different methods for N protein detection; Quantitative determination of N protein in human saliva samples; Characterizations of the probe; Condition optimization experiment data; Probe specificity comparison; MEF mechanism demonstration and some additional figures (PDF)

AUTHOR INFORMATION

Corresponding Authors

Jinpeng Mao − *Department of Chemistry, Tsinghua University, Beijing 100084, P. R. China;* ⦿ orcid.org/0000-0003-3056-6489; Email: jpmao@mail.tsinghua.edu.cn

Sichun Zhang − *Department of Chemistry, Tsinghua University, Beijing 100084, P. R. China;* ⦿ orcid.org/0000-0001-8927-2376; Email: sczhang@mail.tsinghua.edu.cn

Authors

Jie Liu − *Department of Chemistry, Tsinghua University, Beijing 100084, P. R. China*

Mengyu Hou − *Beijing Friendship Hospital, Capital Medical University, Beijing 100050, P. R. China*

Zhian Hu − *Department of Chemistry, Tsinghua University, Beijing 100084, P. R. China*

Gongwei Sun − *Department of Chemistry, Tsinghua University, Beijing 100084, P. R. China; Beijing TASI Technology CO., LTD, Beijing 100085, P. R. China*

Complete contact information is available at:
https://pubs.acs.org/10.1021/acs.analchem.2c02670

Author Contributions

The manuscript was written through contributions of all authors. All authors have given approval to the final version of the manuscript.

Notes

The authors declare no competing financial interest.

ACKNOWLEDGMENTS

REFERENCES

(1) Temmam, S.; Vongphayloth, K.; Baquero, E.; Munier, S.; Bonomi, M.; Regnault, B.; Douangboubpha, B.; Karami, Y.; Chrétien, D.; Sanamxay, D.; Xayaphet, V.; Paphaphanh, P.; Lacoste, V.; Somlor, S.; Lakeomany, K.; Phommavanh, N.; Pérot, P.; Dehan, O.; Amara, F.; Donati, F.; Bigot, T.; Nilges, M.; Rey, F. A.; van der Werf, S.; Brey, P. T.; Eloit, M. *Nature* **2022**, *604*, 330−336.

(2) Chan, J. F.-W.; Yuan, S.; Kok, K.-H.; To, K. K.-W.; Chu, H.; Yang, J.; Xing, F.; Liu, J.; Yip, C. C.-Y.; Poon, R. W.-S.; Tsoi, H.-W.; Lo, S. K.-F.; Chan, K.-H.; Poon, V. K.-M.; Chan, W.-M.; Ip, J. D.; Cai, J.-P.; Cheng, V. C.-C.; Chen, H.; Hui, C. K.-M.; Yuen, K.-Y. *Lancet* **2020**, *395*, 514−523.

(3) Wang, C.; Horby, P. W.; Hayden, F. G.; Gao, G. F. *Lancet* **2020**, *395*, 470−473.

(4) Ortega-Rivera, O. A.; Shin, M. D.; Chen, A.; Beiss, V.; Moreno-Gonzalez, M. A.; Lopez-Ramirez, M. A.; Reynoso, M.; Wang, H.; Hurst, B. L.; Wang, J.; Pokorski, J. K.; Steinmetz, N. F. *J. Am. Chem. Soc.* **2021**, *143*, 14748−14765.

(5) Burke, A. J.; Birmingham, W. R.; Zhuo, Y.; Thorpe, T. W.; Zucoloto da Costa, B.; Crawshaw, R.; Rowles, I.; Finnigan, J. D.; Young, C.; Holgate, G. M.; Muldowney, M. P.; Charnock, S. J.; Lovelock, S. L.; Turner, N. J.; Green, A. P. *J. Am. Chem. Soc.* **2022**, *144*, 3761−3765.

(6) Kong, D.; Wang, X.; Gu, C.; Guo, M.; Wang, Y.; Ai, Z.; Zhang, S.; Chen, Y.; Liu, W.; Wu, Y.; Dai, C.; Guo, Q.; Qu, D.; Zhu, Z.; Xie, Y.; Liu, Y.; Wei, D. *J. Am. Chem. Soc.* **2021**, *143*, 17004−17014.

(7) Chu, D. K. W.; Pan, Y.; Cheng, S. M. S.; Hui, K. P. Y.; Krishnan, P.; Liu, Y.; Ng, D. Y. M.; Wan, C. K. C.; Yang, P.; Wang, Q.; Peiris, M.; Poon, L. L. M. *Clin. Chem.* **2020**, *66*, 549−555.

(8) Xun, G.; Lane, S. T.; Petrov, V. A.; Pepa, B. E.; Zhao, H. *Nat. Commun.* **2021**, *12*, 2905.

(9) Wang, S.; Shu, J.; Lyu, A.; Huang, X.; Zeng, W.; Jin, T.; Cui, H. *Anal. Chem.* **2021**, *93*, 14238−14246.

(10) Amanat, F.; Stadlbauer, D.; Strohmeier, S.; Nguyen, T. H. O.; Chromikova, V.; McMahon, M.; Jiang, K.; Arunkumar, G. A.; Jurczyszak, D.; Polanco, J.; Bermudez-Gonzalez, M.; Kleiner, G.; Aydillo, T.; Miorin, L.; Fierer, D. S.; Lugo, L. A.; Kojic, E. M.; Stoever, J.; Liu, S. T. H.; Cunningham-Rundles, C.; Felgner, P. L.; Moran, T.; Garcia-Sastre, A.; Caplivski, D.; Cheng, A. C.; Kedzierska, K.; Vapalahti, O.; Hepojoki, J. M.; Simon, V.; Krammer, F. *Nat. Med.* **2020**, *26*, 1033−1036.

(11) Yousefi, H.; Mahmud, A.; Chang, D.; Das, J.; Gomis, S.; Chen, J. B.; Wang, H.; Been, T.; Yip, L.; Coomes, E.; Li, Z.; Mubareka, S.; McGeer, A.; Christie, N.; Gray-Owen, S.; Cochrane, A.; Rini, J. M.; Sargent, E. H.; Kelley, S. O. *J. Am. Chem. Soc.* **2021**, *143*, 1722−1727.

(12) Yang, K.; Chaput, J. C. *J. Am. Chem. Soc.* **2021**, *143*, 8957−8961.

(13) Leonard, E. K.; Aller Pellitero, M.; Juelg, B.; Spangler, J. B.; Arroyo-Curras, N. *J. Am. Chem. Soc.* **2022**, *144*, 11226−11237.

(14) van de Plassche, M. A. T.; Barniol-Xicota, M.; Verhelst, S. H. L. *Chembiochem* **2020**, *21*, 3383−3388.

(15) Penalver, L.; Schmid, P.; Szamosvari, D.; Schildknecht, S.; Globisch, C.; Sawade, K.; Peter, C.; Bottcher, T. *Angew. Chem., Int. Ed.* **2021**, *60*, 6799−6806.

(16) Dai, C.; Guo, M.; Wu, Y.; Cao, B. P.; Wang, X.; Wu, Y.; Kang, H.; Kong, D.; Zhu, Z.; Ying, T.; Liu, Y.; Wei, D. *J. Am. Chem. Soc.* **2021**, *143*, 19794−19801.

(17) Kang, H.; Wang, X.; Guo, M.; Dai, C.; Chen, R.; Yang, L.; Wu, Y.; Ying, T.; Zhu, Z.; Wei, D.; Liu, Y.; Wei, D. *Nano Lett.* **2021**, *21*, 7897−7904.

(18) Brodin, P.; Arditi, M. *lancet Gastroentero. Hepatol.* **2022**, *7*, 594−595.

(19) Walls, A. C.; Xiong, X.; Park, Y. J.; Tortorici, M. A.; Snijder, J.; Quispe, J.; Cameroni, E.; Gopal, R.; Dai, M.; Lanzavecchia, A.; Zambon, M.; Rey, F. A.; Corti, D.; Veesler, D. *Cell* **2019**, *176*, 1026−1039.

(20) Sabbih, G. O.; Korsah, M. A.; Jeevanandam, J.; Danquah, M. K. *Biotechnol. Prog.* **2021**, *37*, No. e3096.

(21) Zeng, W.; Ma, H.; Ding, C.; Yang, Y.; Sun, Y.; Huang, X.; He, W.; Xiang, Y.; Gao, Y.; Jin, T. *Signal Transduct Target Ther.* **2021**, *6*, 35.

(22) Kang, S.; Yang, M.; Hong, Z.; Zhang, L.; Huang, Z.; Chen, X.; He, S.; Zhou, Z.; Zhou, Z.; Chen, Q.; Yan, Y.; Zhang, C.; Shan, H.; Chen, S. *Acta Pharm. Sin. B* **2020**, *10*, 1228−1238.

(23) Liu, R.; He, L.; Hu, Y.; Luo, Z.; Zhang, J. *Chem. Sci.* **2020**, *11*, 12157−12164.

(24) Cubuk, J.; Alston, J. J.; Incicco, J. J.; Singh, S.; Stuchell-Brereton, M. D.; Ward, M. D.; Zimmerman, M. I.; Vithani, N.; Griffith, D.; Wagoner, J. A.; Bowman, G. R.; Hall, K. B.; Soranno, A.; Holehouse, A. S. *Nat. Commun.* **2021**, *12*, 1936.

(25) Bai, Z. H.; Cao, Y.; Liu, W. J.; Li, J. *Viruses* **2021**, *13*, 1115.

(26) Zhang, C.; Zhou, L.; Du, K.; Zhang, Y.; Wang, J.; Chen, L.; Lyu, Y.; Li, J.; Liu, H.; Huo, J.; Li, F.; Wang, J.; Sang, P.; Lin, S.; Xiao, Y.; Zhang, K.; He, K. *Front Cell Infect. Microbiol.* **2020**, *10*, 553837.

(27) Zhang, L.; Fang, X.; Liu, X.; Ou, H.; Zhang, H.; Wang, J.; Li, Q.; Cheng, H.; Zhang, W.; Luo, Z. *Chem. Commun.* **2020**, *56*, 10235−10238.

(28) Wang, L.; Wang, X.; Wu, Y.; Guo, M.; Gu, C.; Dai, C.; Kong, D.; Wang, Y.; Zhang, C.; Qu, D.; Fan, C.; Xie, Y.; Zhu, Z.; Liu, Y.; Wei, D. *Nat. Biomed. Eng.* **2022**, *6*, 276−285.

(29) Xu, W.; He, W.; Du, Z.; Zhu, L.; Huang, K.; Lu, Y.; Luo, Y. *Angew. Chem., Int. Ed.* **2019**, *59*, 2−31.

(30) Zhang, H.; Li, F.; Dever, B.; Wang, C.; Li, X. F.; Le, X. C. *Angew. Chem., Int. Ed.* **2013**, *52*, 10698−10705.

(31) Li, F.; Zhang, H.; Lai, C.; Li, X. F.; Le, X. C. *Angew. Chem., Int. Ed.* **2012**, *51*, 9317−9320.

(32) Huang, J.; Zhu, L.; Ju, H.; Lei, J. *Anal. Chem.* **2019**, *91*, 6981−6985.

(33) Li, Q.; Liu, L.; Mao, D.; Yu, Y.; Li, W.; Zhao, X.; Mao, C. *J. Am. Chem. Soc.* **2020**, *142*, 665−668.

(34) Li, M.; Ding, H.; Lin, M.; Yin, F.; Song, L.; Mao, X.; Li, F.; Ge, Z.; Wang, L.; Zuo, X.; Ma, Y.; Fan, C. *J. Am. Chem. Soc.* **2019**, *141*, 18910−18915.

(35) Sun, M.; Liu, S.; Wei, X.; Wan, S.; Huang, M.; Song, T.; Lu, Y.; Weng, X.; Lin, Z.; Chen, H.; Song, Y.; Yang, C. *Angew. Chem., Int. Ed.* **2021**, *60*, 10266−10272.

(36) Schmitz, A.; Weber, A.; Bayin, M.; Breuers, S.; Fieberg, V.; Famulok, M.; Mayer, G. *Angew. Chem., Int. Ed.* **2021**, *60*, 10279−10285.

(37) Zhao, L.; Qi, X.; Yan, X.; Huang, Y.; Liang, X.; Zhang, L.; Wang, S.; Tan, W. *J. Am. Chem. Soc.* **2019**, *141*, 17493−17497.

(38) Wang, J.; Wei, Y.; Hu, X.; Fang, Y. Y.; Li, X.; Liu, J.; Wang, S.; Yuan, Q. *J. Am. Chem. Soc.* **2015**, *137*, 10576−10584.

(39) Yao, G.; Li, J.; Li, Q.; Chen, X.; Liu, X.; Wang, F.; Qu, Z.; Ge, Z.; Narayanan, R. P.; Williams, D.; Pei, H.; Zuo, X.; Wang, L.; Yan, H.; Feringa, B. L.; Fan, C. *Nat. Mater.* **2020**, *19*, 781−788.

(40) Wu, L.; Wang, Y.; Xu, X.; Liu, Y.; Lin, B.; Zhang, M.; Zhang, J.; Wan, S.; Yang, C.; Tan, W. *Chem. Rev.* **2021**, *121*, 12035−12105.

(41) Budhadev, D.; Poole, E.; Nehlmeier, I.; Liu, Y.; Hooper, J.; Kalverda, E.; Akshath, U. S.; Hondow, N.; Turnbull, W. B.; Pohlmann, S.; Guo, Y.; Zhou, D. *J. Am. Chem. Soc.* **2020**, *142*, 18022−18034.

(42) Shi, L.; Wang, L.; Ma, X.; Fang, X.; Xiang, L.; Yi, Y.; Li, J.; Luo, Z.; Li, G. *Anal. Chem.* **2021**, *93*, 16646−16654.

(43) Wang, D.; He, S.; Wang, X.; Yan, Y.; Liu, J.; Wu, S.; Liu, S.; Lei, Y.; Chen, M.; Li, L.; Zhang, J.; Zhang, L.; Hu, X.; Zheng, X.; Bai, J.; Zhang, Y.; Zhang, Y.; Song, M.; Tang, Y. *Nat. Biomed. Eng.* **2020**, *4*, 1150−1158.

(44) Deng, H.; Yan, S.; Huang, Y.; Lei, C.; Nie, Z. *TrAC Trends in Anal. Chem.* **2020**, *122*, 115757.

(45) Montes-Garcia, V.; Squillaci, M. A.; Diez-Castellnou, M.; Ong, Q. K.; Stellacci, F.; Samori, P. *Chem. Soc. Rev.* **2021**, *50*, 1269−1304.

(46) Sundaresan, S. M.; Fothergill, S. M.; Tabish, T. A.; Ryan, M.; Xie, F. *Applied Phys. Rev.* **2021**, *8*, 041311.

(47) Liu, Y.; Tuleouva, N.; Ramanculov, E.; Revzin, A. *Anal. Chem.* **2010**, *82*, 8131−8136.

(48) Liu, Y.; Yan, J.; Howland, M. C.; Kwa, T.; Revzin, A. *Anal. Chem.* **2011**, *83*, 8286−8292.

(49) Tuleuova, N.; Jones, C. N.; Yan, J.; Ramanculov, E.; Yokobayashi, Y.; Revzin, A. *Anal. Chem.* **2010**, *82*, 1851−1857.

(50) Fredriksson, S.; Gullberg, M.; Jarvius, J.; Olsson, C.; Pietras, K.; Gustafsdottir, S. M.; Ostman, A.; Landegren, U. *Nat. Biotechnol.* **2002**, *20*, 473−477.

(51) Schallmeiner, E.; Oksanen, E.; Ericsson, O.; Spangberg, L.; Eriksson, S.; Stenman, U. H.; Pettersson, K.; Landegren, U. *Nat. Methods* **2007**, *4*, 135−137.

(52) Ziegler, C. G. K.; Allon, S. J.; Nyquist, S. K.; Mbano, I. M.; Miao, V. N.; Tzouanas, C. N.; Cao, Y.; Yousif, A. S.; Bals, J.; Hauser, B. M.; Feldman, J.; Muus, C.; Wadsworth, M. H.; Kazer, S. W.; Hughes, T. K.; Doran, B.; Gatter, G. J.; Vukovic, M.; Taliaferro, F.; Mead, B. E.; Guo, Z.; Wang, J. P.; Gras, D.; Plaisant, M.; Ansari, M.; Angelidis, I.; Adler, H.; Sucre, J. M. S.; Taylor, C. J.; Lin, B.; Waghray, A.; Mitsialis, V.; Dwyer, D. F.; Buchheit, K. M.; Boyce, J. A.; Barrett, N. A.; Laidlaw, T. M.; Carroll, S. L.; Colonna, L.; Tkachev, V.; Peterson, C. W.; Yu, A.; Zheng, H. B.; Gideon, H. P.; Winchell, C. G.; Lin, P. L.; Bingle, C. D.; Snapper, S. B.; Kropski, J. A.; Theis, F. J.; Schiller, H. B.; Zaragosi, L. E.; Barbry, P.; Leslie, A.; Kiem, H. P.; Flynn, J. L.; Fortune, S. M.; Berger, B.; Finberg, R. W.; Kean, L. S.; Garber, M.; Schmidt, A. G.; Lingwood, D.; Shalek, A. K.; Ordovas-Montanes, J. *Cell* **2020**, *181*, 1016−1035.